Electromagnetic Investigation of Shielding Effect of NI REBCO Windings on Screening Current Distribution Change

Takanobu Mato, *Member, IEEE*, Jeseok Bang, Atsushi Ishiyama, and So Noguchi, *Member, IEEE*

***Abstract*—Techniques for high field generation have been advancing. No-insulation (NI) rare-earth barium copper oxide (REBCO) pancake coils enable high field generations with high thermal stability. One of the major challenges in REBCO magnet development is the screening current reduction. The screening current is induced in the REBCO tape by the change of the field perpendicular to the REBCO tape surface. It deteriorates the field, sometimes together with mechanical stability. Since the behaviors of the screening current are clear by simulations, it is important to consider the screening current effect in the design stage to reduce it or control the coil performances. In this paper, we explore the effectiveness of the non-energized coil (hereafter called "dummy coil") to modify the screening current distribution. The dummy coils are wound employing the NI winding technique. The electromagnetic behaviors of the insert NI REBCO magnet that consists of 12 stacked single pancake coils with a few dummy coils are investigated through the electromagnetic simulation with the finite element method (FEM). The results show that the dummy coils can suppress the variance of the current density distribution, although there is a trade-off with respect to field reduction.**

***Index Terms*—FEM, no-insulation REBCO magnet, non-energized winding, screening current distribution.**

I. Introduction

THE no-insulation (NI) rare-earth barium copper oxide (REBCO) is a promising candidate for high field generation [1]. Its applications spread to a wide area: nuclear magnetic resonance (NMR) [2], magnetic resonance imaging (MRI) [3], particle accelerator [4], and nuclear fusion reactor [5]. The NI winding technology eliminates the insulation between turns, and it significantly improves the thermal stability of the REBCO coils. As the behaviors of the NI REBCO coils have been clarified through simulations and experiments [6], [7], [8], the NI REBCO coil is one of the good options for high field generation.

Received 27 July 2025; revised 6 October 2025; accepted 20 October 2025. Date of publication 24 October 2025; date of current version 6 November 2025. This work was supported by the JSPS KAKENHI under Grant 25K17589. *(Corresponding author: Takanobu Mato.)*

Takanobu Mato and So Noguchi are with the Graduate School of Information Science and Technology, Hokkaido University, Sapporo 060-0814, Japan (e-mail: mato@ist.hokudai.ac.jp; noguchi@ssi.ist.hokudai.ac.jp).

Jeseok Bang is with the National High Magnetic Field Laboratory, Tallahassee, FL 32310 USA.

Atsushi Ishiyama is with the Waseda University, Tokyo 169-8555, Japan.

Color versions of one or more figures in this article are available at https://doi.org/10.1109/TASC.2025.3625522.

Digital Object Identifier 10.1109/TASC.2025.3625522

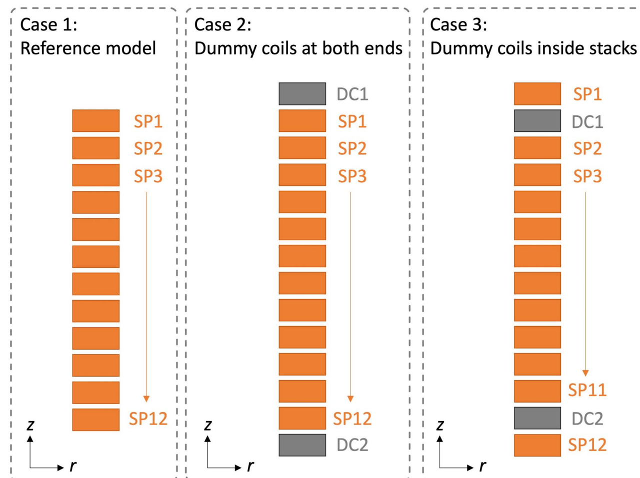

Fig. 1. Three cases of insert coils simulated in this paper. Dummy coils are denoted as DCs, while single pancake coils are SPs.

One of the main issues in the high field generation by REBCO coils is the screening current [9]. The screening current is induced by the field perpendicular to the REBCO tape surface; e.g., during the REBCO magnet charge and discharge. The screening current distorts the field distribution, and both spatial and temporal field homogeneity are deteriorated [10], [11]. Another aspect of the screening current is a local high stress [12]. A large current is induced on the edges of REBCO tapes during magnet charge, subjecting the REBCO tapes to complex and intense electromagnetic forces. Several experiments in high field generation test results showed the plastic deformations of REBCO tapes [13]. It is considered that the screening current-induced stress is probably one of the causes of quenches in the high field REBCO magnets [14], [15].

Some methods have been proposed to address the screening current reduction: 1) current control [16], [17], 2) temperature control [18], [19], 3) conductor and geometry design [20], and 4) charging sequence [21]. These methods are based on either reduction of the radial field penetrating the wide surface of REBCO tapes or acceleration of the tape-transverse current diffusion in REBCO layers. It is widely accepted that an appropriate method should be chosen depending on applications considering its pros/cons. Expanding the range of available methods is important as it directly translates into flexibility in magnet design.

TABLE I
COIL SPECIFICATIONS AND OPERATION PARAMETERS

Parameters	Values
REBCO tape width [mm]	4.0
REBCO tape thickness [mm]	0.1
Inner diameter [mm]	30
Outer diameter [mm]	50
Number of turns	100
Pancake spacing [mm]	1.0
Winding method	no-insulation
Contact resistivity [μΩ·cm^2]	70
Contact resistance [mΩ]	167
Inductance (Case1) [mH]	23.37
I_{c0} [A]	3500
B_0 [T]	0.9
α	0.6
n-index value	25

In this paper, we would rather focus on changing the current distribution of the NI REBCO coils by placing the additional NI REBCO windings not energized. Hereafter, this winding is referred to as the "dummy coil." The dummy coils change the field distribution and the consequent current distribution of the NI REBCO coils. In the paper, we show the results of simple cases as a first step for the technique in current distribution modification: the dummy coils are placed at the coil stack end or between the REBCO pancake coils. The electromagnetic simulation coupling with the finite element method (FEM) and the circuit analysis is performed to investigate the electromagnetic behaviors of NI REBCO single pancake (SP) coil stack with a few dummy coils. The current distribution and the reduction of the field are discussed.

II. SIMULATION MODEL

A. Simulation Cases

We have simulated the electromagnetic behaviors of an insert NI REBCO magnet positioned inside a resistive outsert magnet. The insert NI REBCO magnet consists of 12 stacked single pancake coils and 2 dummy coils. Fig. 1 shows the three insert coils subjected to simulation. Case 1 is the reference model, in which 12 single pancake coils (SP1 to SP12) are simply stacked without dummy coil. Case 2 has 2 dummy coils (DC1 and DC2) at both top and bottom ends of the stack. Whereas, in Case 3, the dummy coils are inserted one SP coil inward to the magnet center. It is noted that the dummy coils are wound without turn-to-turn insulation and not electrically connected to the SP coils charged.

The magnet specifications are listed in Table I. Each single pancake coil has 100 turns and the inductance of the insert stacked SP magnet is 23.4 mH in Case 1. The contact resistivity of 70 μΩ·cm^2 is used for all SPs and DCs [22]. In the simulation, the index model is employed to compute the virtual REBCO conductivity. The critical current J_c is calculated with Kim model to consider the field dependence, as shown in the following equation [23]:

$$J_c = \frac{I_{c0}}{S\left(1+\frac{|B|}{B_0}\right)^{\alpha}}, \tag{1}$$

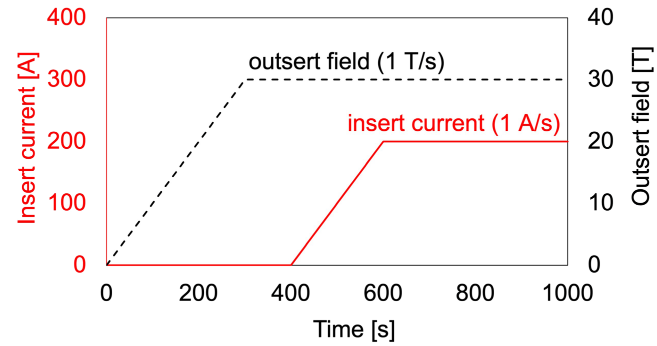

Fig. 2. Operation of magnet. Field by the outsert magnet is first charged to 30 T at 1 T/s, followed by the insert magnet to 200 A with ramp speed of 1 A/s.

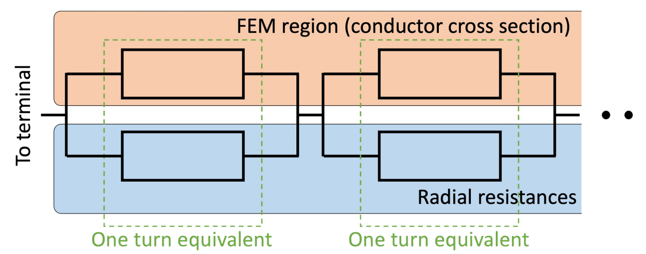

Fig. 3. Circuit representing FEM conductor region and radial resistance.

where S is the REBCO conductor cross-sectional area and $\boldsymbol{B}$ is the field. The parameters I_{c0}, B_0, and α are shown in Table I.

The insert REBCO magnet is assumed to be operated at liquid helium temperature. Fig. 2 presents the magnet charging sequence.

B. Electromagnetic Simulation

The electromagnetic simulation is performed to compute the current density distribution of the NI REBCO SP coil stack. The $A-\phi$ formulation is used in this paper. The governing equation is given as follows:

$$\nabla \times \frac{1}{\mu_0}\nabla \times A = J_0 - \sigma\left(\frac{\partial A}{\partial t} + \nabla\phi\right), \tag{2}$$

$$\nabla \cdot \left\{\sigma\left(\frac{\partial A}{\partial t} + \nabla\phi\right)\right\} = 0, \tag{3}$$

where A, ϕ, μ_0, σ, and J_0 is the magnetic vector potential, the electric scalar potential, the permeability of free space, the electrical conductivity, and the current density corresponding to the operating current, respectively. The above (2) and (3) are solved for the current vector potential in the whole domain and the scalar potential in the superconducting domain. The net current density J is obtained as

$$J = J_0 + \nabla \cdot \left\{\sigma\left(\frac{\partial A}{\partial t} + \nabla\phi\right)\right\}. \tag{4}$$

The governing equations are formulated with the FEM to obtain the distribution of the current density and magnetic field. The FEM is coupled with an electric circuit to represent the radial currents of the NI REBCO coils as shown in Fig. 2. One turn is modeled with the FEM conductor having the radial resistance (a

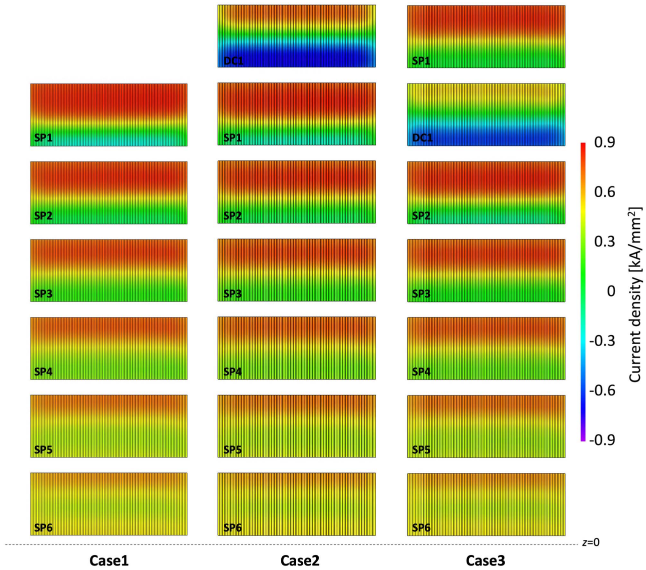

Fig. 4. Azimuthal current density distribution of Case 1, 2, and 3 at $t = 1000$ s. Upper half of the insert is shown.

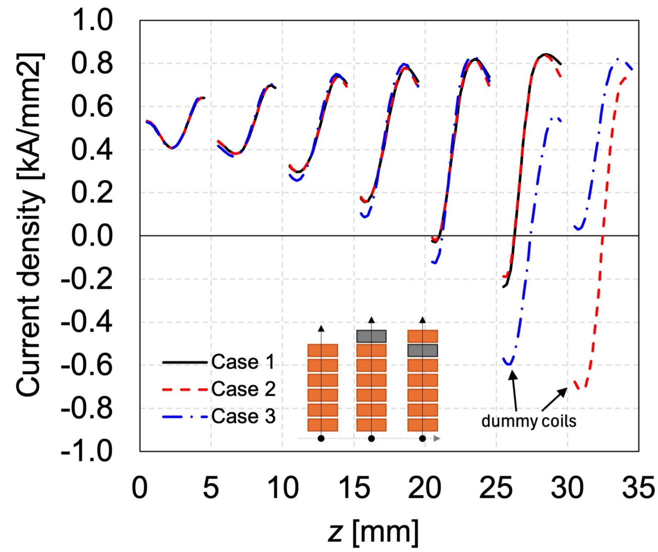

Fig. 5. Current density on a line at middle of pancake thickness (at $r = 20$ mm). The line on where the current density is plotted is also shown together with coil geometries. The dummy coil homogenizes the distribution of the current density of SP1 in Case 3.

turn-to-turn contact resistance) connected in parallel. The FEM conductor corresponds to one turn, while the radial resistance R_{r} is obtained using the equation below:

$$R_{\mathrm{r}} = \frac{\rho_{\mathrm{r}}}{2\pi r w}\ , \tag{5}$$

where ρ_{r}, r, and w are the radial turn-to-turn contact resistivity, the r-coordinate of winding, and the REBCO tape width, respectively.

It is noted that the simulation region is reduced to an upper half using a symmetry boundary at $z = 0$. The magnetic field generated with the outsert magnet is represented as a uniform background field. The design value of the central axial field is 34.12 T for Cases 1 and 2, and 34.05 T for Case 3.

We used the commercial software JMAG and the aforementioned formulations are available as a standard superconductor function [24].

III. Simulation Results

A. Azimuthal Current Density Distribution

Fig. 4 shows the current density distribution of three cases at $t = 1000$ s, where only the upper half (SP1 to SP6) is depicted. In Case 1, the screening current is largely induced in SP1, penetrating to approximately the middle of the REBCO tape width. This is because SP1 experiences the largest radial field fluctuations among the other SPs in Case 1.

In Case 2, the dummy coil (DC1) is placed above the SP1. The current density distributions of SPs are almost indistinguishable from those of Case 1. In contrast, the dummy coil shows a largely different current distribution from SPs. The positive-directional current flows on the top edge, and the negative-directional current is induced on the bottom edge. This is because SP1 generates a large magnetic field directing radially outward at DC1, and the screening current is induced in DC1 so that the radial field is shielded.

In Case 3, the current distribution of SP1 appears different from the previous two cases. The penetration depth of the screening current in SP1 seems shorter than in the other cases. Another point to note is that the negative-directional current on the lower edge does not appear in SP1 (detailed later). The screening current is also induced in DC1; however, the maximum and minimum current density values are relatively small compared with Case 2 because DC1 in Case 3 experiences less change in the radial field.

To detail more quantitatively, the current density of each case on a line at $r = 20$ mm (at the middle of the SP thickness) across the coil height is shown in Fig. 5. It is obviously shown that SP1 in Case 3 (the blue dash-dotted line on the most right) has no negative-directional current, while SP1s in Cases 1 and 2 (the black solid and the broken red lines between 25-30 mm, respectively) have the negative-directional currents. It indicates that the dummy coil effectively works, resulting in a more uniform current density distribution across the tape width.

One of the benefits of the uniform current distribution is the uniformity of the screening current-induced stress. The uniform stress distribution may lead to better effectiveness of the over-bandings to mitigate the screening current-induced stress. Also, given that the screening current-induced stress occurs at the lower edge of the coil due to the complicated stress state, i.e., a combination of the tape rotation and the compression forces, reducing or suppressing the negative-directional screening current is effective [25]. In Fig. 5, the lower edge current of SP1 is -0.24 kA/mm^2 in Case 1, and this is reduced to 0.04 kA/mm^2 in Case 3. It needs further validation by computing the mechanical behaviors coupled with the electromagnetic simulation.

It is also noteworthy that the dummy coil location is important. Table II compares the difference of maximum current density

TABLE II
COMPARISON OF $J_{MAX} - J_{MIN}$

[kA/mm²]	Case 1	Case 2	Case 3
SP1	1.077	1.026	0.792
SP2	0.849	0.838	0.956
SP3	0.624	0.616	0.710
SP4	0.443	0.437	0.495
SP5	0.317	0.313	0.335
SP6	0.233	0.231	0.241

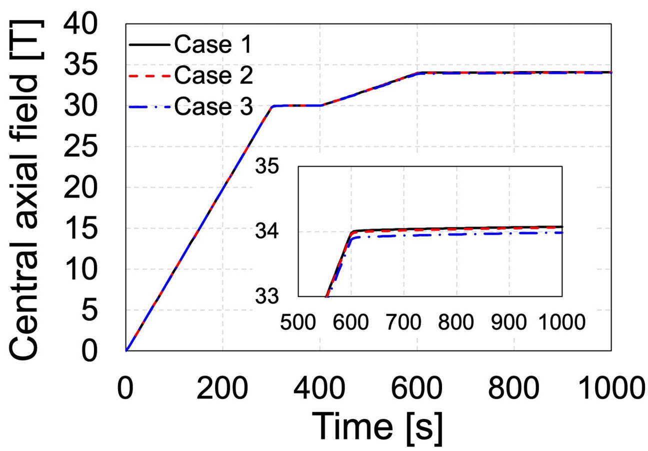

Fig. 6. Axial field at magnet center during magnet charge. The inset shows the enlarged plot at the end of the insert charge.

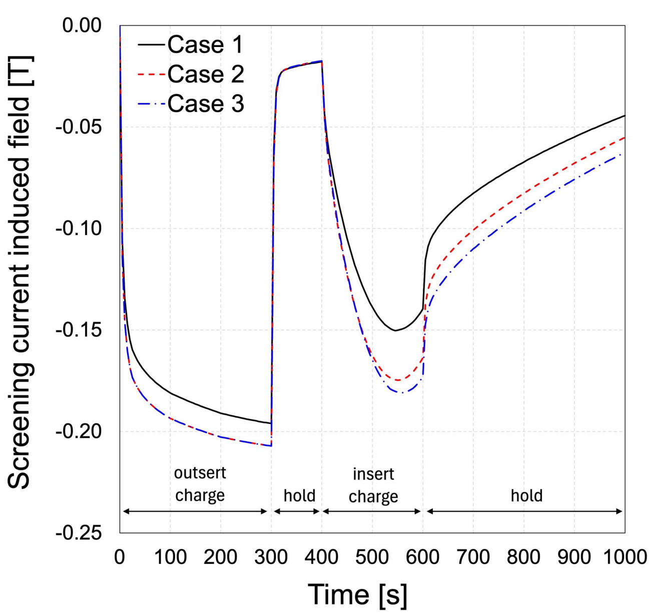

Fig. 7. Screening current induced field during magnet charge. The dummy coil increases the screening current induced field.

$J_{\max}$ and minimum current density $J_{\min}$ on the same position in Fig. 5 for each SPs. The comparison of Cases 1 and 3 reveals that the current density is homogenized only in SP1, whereas the difference is slightly increased in SP2. This is because the current on the lower edge of the dummy coil generates the radially outward field on SP2, inducing more screening current.

B. Effect on Field

Next, we investigate the effect of the dummy coils on the field. Fig. 6 shows the axial field at the magnet center. The field increases almost proportionally to the current and the external field generated by the outsert magnet. The effect of the no-insulation winding, i.e., the significant field delay, is not observed because the time constant of the magnet is 0.14 s. The enlargement view shows the axial field after the charge of the inset REBCO magnet. The axial fields of Cases 1 and 2 are almost identical since all the SPs are located at the same position. The axial field of Case 3 has a slightly lower field intensity than the other cases, merely due to the lower designed field.

Now, we compare the screening current-induced field (SCIF) B_{SCIF} which is defined as follows:

$$B_{\mathrm{SCIF}} = B_{\mathrm{sim}} - B_{\mathrm{uni}}, \tag{6}$$

where B_{sim} is the axial field obtained from the screening current simulation, and B_{uni} is the axial field generated by the uniform current distribution, respectively. The temporal SCIF variation is shown in Fig. 7. Since the NI REBCO insert is magnetically coupled with the outsert magnet, a significant amount of the SCIF is observed during the outsert magnet charge, and then it attenuates in a short time on the following hold operation. In the insert REBCO magnet charging and the subsequent hold operation, the SCIF of Case 3 is the largest. At $t = 1000$ s, Case 3 exhibits approximately 41% higher SCIF value and 24% for Case 2, when compared with Case 1.

It is evident that the presence of additional superconducting regions leads to the field reduction. The SCIF needs to be carefully evaluated when the dummy coils are applied.

IV. CONCLUSION

In this paper, we propose the dummy coil (DC), which is merely the no-insulation (NI) RBECO windings not connected to a power source. The finite element analysis based on the $A - \phi$ formulation coupled with the electric circuit representing the radial current paths is performed to compute the electromagnetic behaviors of the NI REBCO single pancake coil stack inside the outsert magnet. The simulation results reveal that the dummy coil inserted between SP1 and SP2 (corresponding to Case 3) mitigates the distributed current density in SP1, although the screening current-induced field is increased. It implies the screening current-induced stress could be mitigated because the electromagnetic force is more uniformly applied, and the stress would be well-shared with the windings and the over-bandings. It needs to be validated through the mechanical simulation in the near future. Another possible advantage of the dummy coils is the protection of the pancake coil from the normal-state transitions. Some of the energy dissipates in the dummy coil and possibly works as a magnetic dam [26], [27].

ACKNOWLEDGMENT

The authors would like to thank Yohei Watanabe, JSOL Corporation and Hirokatsu Katagiri, JSOL Corporation for their assistance in JMAG simulation.

REFERENCES

[1] S. Hahn, D. K. Park, J. Bascuñán, and Y. Iwasa, "HTS pancake coils without turn-to-turn insulation," *IEEE Trans. Appl. Supercond.*, vol. 21, no. 3, pp. 1592–1595, Jun. 2011.

[2] B. Parkinson et al., "Design and manufacture of an ultra-compact, 1.5 T class, controlled-contact resistance, REBCO, brain imaging MRI magnet," *Supercond. Sci. Technol.*, vol. 37, no. 11, 2024, Art. no. 115026.

[3] J. Bascuñán, S. Hahn, D. K. Park, and Y. Iwasa, "A 1.3-GHz LTS/HTS NMR magnet – A progress report," *IEEE Trans. Appl. Supercond.*, vol. 21, no. 3, pp. 2092–2095, Jun. 2011.

[4] M. Durante, P. Fazilleau, T. Lecrevisse, C. Lorin, M. Segreti, and O. Tellier, "Overview of HTS accelerator magnet developments at CEA saclay," *IEEE Trans. Appl. Supercond.*, vol. 34, no. 5, Aug. 2024, Art. no. 4002905.

[5] Z. S. Hartwig et al., "The SPARC toroidal field model coil program," *IEEE Trans. Appl. Supercond.*, vol. 34, no. 2, Mar. 2024, Art. no. 0600316.

[6] A. Ikeda et al., "Transient behaviors of no-insulation REBCO pancake coil during local normal-state transition," *IEEE Trans. Appl. Supercond.*, vol. 26, no. 4, Jun. 2016, Art. no. 4600204.

[7] X. Wang, T. Wang, E. Nakada, A. Ishiyama, R. Itoh, and S. Noguchi, "Charging behavior in no-insulation REBCO pancake coils," *IEEE Trans. Appl. Supercond.*, vol. 25, no. 3, Jun. 2015, Art. no. 4601805.

[8] K. R. Bhattarai, K. Kim, S. Kim, S. Lee, and S. Hahn, "Quench analysis of a multiwidth no-insulation 7-T 78-mm REBCO magnet," *IEEE Trans. Appl. Supercond.*, vol. 27, no. 4, Jun. 2017, Art. no. 4603505.

[9] D. Kolb-Bond et al., "Screening current rotation effects: SCIF and strain in REBCO magnets," *Supercond. Sci. Technol.*, vol. 34, no. 9, 2021, Art. no. 095004.

[10] H. Ueda, M. Fukuda, K. Hatanaka, T. Wang, A. Ishiyama, and S. Noguchi, "Spatial and temporal behavior of magnetic field distribution due to shielding current in HTS coil for cyclotron application," *IEEE Trans. Appl. Supercond.*, vol. 23, no. 3, Jun. 2013, Art. no. 4100805.

[11] H. Ueda et al., "Numerical simulation on magnetic field generated by screening current in 10-T-class REBCO coil," *IEEE Trans. Appl. Supercond.*, vol. 26, no. 4, Jun. 2016, Art. no. 4701205.

[12] H. Ueda, K. Naito, R. Inoue, and S. Kim, "Deformation analysis of no-insulation REBCO coils considering turn-to-turn contact configuration," *IEEE Trans. Appl. Supercond.*, vol. 32, no. 6, Sep. 2022, Art. no. 4604205.

[13] X. Hu et al., "Analyses of the plastic deformation of coated conductors deconstructed from ultra-high field test coils," *Supercond. Sci. Technol.*, vol. 33, 2020, Art. no. 095012.

[14] J. Bang et al., "Evidence that transverse variability of critical current density can greatly mitigate screening current stress in high field REBCO magnets," *Sci. Rep.*, vol. 14, no. 1, 2024, Art. no. 31703.

[15] S. Takahashi et al., "Hoop stress modification, stress hysteresis and degradation of a REBCO coil due to the screening current under external magnetic field cycling," *IEEE Trans. Appl. Supercond.*, vol. 30, no. 4, Jun. 2020, Art. no. 4602607.

[16] Y. Yanagisawa et al., "Effect of coil current sweep cycle and temperature change cycle on the screening current-induced magnetic field for YBCO-coated conductor coils," in *Proc. AIP Conf.*, vol. 1434, no. 1, pp. 1373–1380, 2012.

[17] Y. Nagasaki et al., "Influence of preexcitation, high temperature magnetization and combined excitation method on screening current attenuation in conduction-cooled REBCO coil," *IEEE Trans. Appl. Supercond.*, vol. 30, no. 5, Aug. 2020, Art. no. 4401006.

[18] J. Bang et al., "A customized electric heater to mitigate screening current by optimal control on temperature distribution in a high-temperature superconductor coil," *J. Appl. Phys.*, vol. 132, no. 18, 2022, Art. no. 183911.

[19] W. Lee, D. Park, J. Bascuñán, and Y. Iwasa, "Construction and test result of an All-REBCO conduction-cooled 23.5 T magnet prototype towards a benchtop 1 GHz NMR spectroscopy," *Supercond. Sci. Technol.*, vol. 35, no. 10, 2022, Art. no. 105007.

[20] A. C. Wulff, A. B. Abrahamsen, and A. Insinga, "Topical review: Multifilamentary coated conductors for ultra-high magnetic field applications," *Supercond. Sci. Technol.*, vol. 34, no. 5, 2021, Art. no. 053003.

[21] L. Shao et al., "Reduction of screening-current induced strain in REBCO coils via preferential generation of perpendicular field during charging," *Supercond. Sci. Technol.*, vol. 38, no. 6, 2025, Art. no. 065022.

[22] X. Wang et al., "Turn-to-turn contact characteristics for an equivalent circuit model of no-insulation ReBCO pancake coil," *Supercond. Sci. Technol.*, vol. 26, no. 3, 2013, Art. no. 035012.

[23] B. C. Robert, M. U. Fareed, and H. S. Ruiz, "How to choose the superconducting material law for the modelling of 2G-HTS coils," *Materials*, vol. 12, no. 17, 2019, Art. no. 2679.

[24] JMAG, Accessed: Jul. 25, 2025. [Online]. Available: https://www.jmag-international.com/

[25] J. Park et al., "Numerical study on effect of boundary conditions and winding compressibility on screening current induced stress," *IEEE Trans. Appl. Supercond.*, vol. 35, no. 5, Aug. 2025, Art. no. 4801805.

[26] S. An et al., "A feasibility study on 'magnetic dam' to absorb magnetic energy in NI HTS magnet during quench," *IEEE Trans. Appl. Supercond.*, vol. 30, no. 4, Jun. 2020, Art. no. 4701705.

[27] T. Mato and S. Noguchi, "Effect comparison of different conductor widths in magnetic dam for protection of NI REBCO pancake coils," *IEEE Trans. Appl. Supercond.*, vol. 34, no. 3, May 2024, Art. no. 4701705.